Local magnetism and structural properties of Heusler Ni_2MnGa alloys

M. Belesi,[1,*] L. Giebeler,[1] C. G. F. Blum,[1] U. K. Rößler,[1] B. Büchner,[1,2] and S. Wurmehl[1,2,†]
[1]*Leibniz Institute for Solid State and Materials Research, Helmholtzstrasse 20, 01069 Dresden, Germany*
[2]*Institute for Solid State Physics, TU Dresden D-01069, Germany*
(Received 28 November 2013; revised manuscript received 29 March 2015; published 13 April 2015)

We present a detailed experimental study of bulk and powder samples of the ferromagnetic Heusler shape-memory alloy Ni_2MnGa, including zero-field static and dynamic ^{55}Mn NMR experiments, x-ray powder diffraction and magnetization experiments. The NMR spectra give direct access to the sequence of structural phase transitions in this compound, from the high-T austenitic phase down to the low-T martensitic phase. In addition, a detailed investigation of the so-called *rf*-enhancement factor delivers the local magnetic stiffness and restoring fields for each separate structural environment, thus, differentiating signals coming from austenitic and martensitic components. In this way we can also resolve differences in the local spin moments of the two phases of the order of 0.08 Bohr magnetons, and reveal precursor phenomena of the martensitic transformation well inside the parent austenitic phase.

DOI: 10.1103/PhysRevB.91.134415 PACS number(s): 76.60.Jx, 75.50.Cc

I. INTRODUCTION

The discovery of a martensitic phase transition in Ni_2MnGa below the ferromagnetic (FM) Curie point by Webster *et al.* in 1984 [1] has triggered an extensive experimental and theoretical activity on Heusler and related alloys over the last three decades [2,3]. Besides their fundamental interest, the complex interplay of structural, magnetic, and electronic degrees of freedom in these compounds gives rise to technologically functional properties such as magnetic shape memory [4], magnetocaloric [5], as well as magnetoresistance effects [6].

Ni_2MnGa is a FM Heusler alloy with Curie temperature $T_c \simeq 380$ K [1]. The magnetic moment is mainly localized on Mn sites, while the Ni moments are much smaller (a tenth of the Mn moment) [1]. Still, the conduction electrons from Ni seem to play an important role in mediating the Mn-Mn interactions and the ferromagnetic ordering in Ni_2MnGa [7].

Upon cooling below T_c, Ni_2MnGa shows two thermally driven structural transitions, one from the high-temperature austenitic to the so-called premartensitic (PM) phase at $T_{PM} \simeq 260$ K, and another from the PM to the martensitic phase at $T_M \simeq 200$ K [1]. In the austenitic phase, Ni_2MnGa has the fcc $L2_1$ crystal structure with $a = 5.825$ Å and space group (SG) $Fm\bar{3}m$ (No. 225) [1]. The PM transition proceeds via a pronounced softening in the $[\zeta\zeta 0]$ TA_2 phonon branch at $\zeta = 1/3$, as observed by inelastic neutron scattering (INS) measurements reported by Zheludev *et al.* [8]. The freezing of the displacements associated with this softening gives rise to a distortion of the austenitic structure with the propagation vector of the soft mode [8]. This softening, which has also been observed in other shape-memory alloys with similar structure [9,10], can be ascribed to the interplay of strong electron-phonon coupling and Fermi surface (FS) nesting [11–15] (see also the phenomenological model by Planes *et al.* [16] and the first-principles calculations by Uijttewaal *et al.* [17]). Besides the structural modifications [8,18–20], the PM transition is also accompanied by small field-dependent magnetization changes at T_{PM} [21].

Turning to the martensitic phase below $T_M \simeq 200$ K [1], its crystal structure and space group remain under debate. The martensitic phase has been described as a nearly tetragonal [1,18] or orthorhombic [22,23] distortion of the parent cubic phase, with an additional long-wavelength modulation along the c axis. Martynov *et al.* [24] reported that the superstructure can be described as a periodic shuffling of the (100) planes along the $[\bar{1}00]$ direction with a period of five atomic layers [fivefold modulation (5M)], while neutron scattering experiments by Zheludev *et al.* [18] point to an incommensurate wave vector (0.43,0.43,0) close to the 5M structure. A similar incommensurate modulation vector was also reported by Righi *et al.* [23] based on x-ray powder diffraction experiments, and more recently by the single-crystal study of Mariager *et al.* [25]. On the other hand, Brown *et al.* [22] inferred that the martensitic phase is commensurate 7M with orthorhombic symmetry and SG *Pnnm* (No. 58), while recent high-resolution synchrotron x-ray powder diffraction measurements by Singh *et al.* [26], show an orthorhombic symmetry and an incommensurate modulation with an approximate 7M structure. Finally, we should remark that some of these structural differences may originate in sample preparation details [27,28] and can be sensitive to stoichiometry [2,3].

Besides the exact crystal structure of the martensitic phase, the microscopic origin of the martensitic transition is also debated, the main proposals being the band Jahn-Teller mechanism [29–32] on one hand, and strong electron phonon-coupling and FS nesting [8,18] on the other. The latter has been supported by extended *ab initio* calculations, which have succeeded into reproducing several experimental findings [13–15]. Recent neutron scattering experiments by Shapiro *et al.* [33], reported well-defined phason excitations, which were associated to the charge density wave (CDW) resulting from FS nesting [14]. Furthermore, ultraviolet-photoemission measurements have shown the formation of a pseudogap 0.3 eV below the Fermi energy at T_{PM} [34,35], which has also been attributed to CDW due to the FS

*m.e.belesi@ifw-dresden.de
†s.wurmehl@ifw-dresden.de

nesting [31]. A third proposal for the explanation of complex lattice structures in shape-memory materials is the concept of adaptive martensites [36], which was recently applied to Ni_2MnGa [37]. In this scenario, the stabilization of long-period modulated and incommensurate phases is not of electronic origin, instead they are metastable nanoscale microstructures formed from variants of the stable tetragonal phase.

Here we present a zero-field static and dynamic ^{55}Mn NMR study of bulk and powder samples of Ni_2MnGa alloy, complemented by magnetization and x-ray powder diffraction experiments. The NMR experiments provide local access to the above mentioned sequence of structural phase transitions from the high-T austenitic to the premartensitic and finally to the low-T martensitic phase. In addition, a detailed study of the so-called *rf*-enhancement factors allows to probe the stiffness and local anisotropy for each separate magnetic environment. In this way, we are able to differentiate the signals from the austenitic and martensitic components and follow their evolution with temperature. Our measurements on bulk and powdered samples demonstrate strong dependence on sample preparation.

The article is organized as follows. In Sec. II we provide the experimental details. In Sec. III A we present the x-ray powder diffraction experiments. In Sec. III B we present our magnetization measurements and in Sec. III C the NMR results. A brief summary of our results is finally given in Sec. IV.

II. EXPERIMENTAL DETAILS

Polycrystalline samples of Ni_2MnGa were prepared by the repeated arc melting of stoichiometric quantities of the starting elements in an arc discharge furnace. The resulting ingot was annealed for homogenization at 800 °C for two weeks and later was cut in two pieces. Hereafter, we will call the first piece of the ingot "sample I". The second piece of the ingot was crushed into powder and will be referred to as "sample II" in the following. Both samples were studied by magnetization and NMR measurements, while sample II was also studied by x-ray powder diffraction at room temperature. Upon completing these experiments sample II was sealed under low argon pressure in a quartz ampule, and annealed for four days at 600 °C. The ampule was subsequently quenched in iced water. This procedure was repeated one more time. We will refer to the annealed sample produced by the aforementioned process as "sample III". In this particular sample we have performed, apart from the magnetization and NMR experiments, x-ray powder diffraction experiments as a function of temperature.

The x-ray powder diffraction experiments were performed on a STOE Stadi P powder diffractometer with Mo $K_{\alpha 1}$ radiation. Sample II was studied at 293 K, and sample III between 140–293 K. The diffractometer is equipped with a curved Ge(111) monochromator and a 6° linear position sensitive detector. Sample II was measured in transmission geometry as flat sample with a thin powder layer glued onto a polyacetate film. Sample III was filled in a capillary, which was afterwards sealed and measured in Debye-Scherrer mode with a step size of 0.01° and 100 s/step in the range $15^\circ \leqslant 2\theta \leqslant 60^\circ$. The data were evaluated by the Rietveld method [38] with Fullprof in the WinPlotR program package [39]. For $T \geqslant 170$ K mainly the austenitic phase, SG $Fm\bar{3}m$ [40], was used as structure model. For 140 K $< T \leqslant 200$ K, the 7M in-phase model with SG *Pnnm* [41] was taken as second phase, while at $T = 140$ K only the latter. For the refinements, a Thompson-Cox-Hastings pseudo-Voigt profile function was selected [42]. As refinable parameters background, scale factor, half width, Caglioti variables (U, V, W), lattice parameters, asymmetries and the overall temperature factor B_{ov} were allowed. For cooling, an Oxford Cryosystems 700 series equipment was used to cycle the sample within a temperature range of 140–293 K. At every temperature, the sample was equilibrated for 1 h before starting the measurement.

The magnetization measurements were performed with a SQUID magnetometer (MPMS, Quantum Design) in the temperature range of 2–400 K and for applied fields up to 5 T. The temperature dependence of the magnetization was measured in zero-field cooling (ZFC) and in field cooling (FC) modes. In the ZFC mode, the sample was first cooled to 2 K in zero field, then a magnetic field was applied and the data were collected while heating. In the field cooled (FC) measurements, the magnetic field was applied above the transition temperature to the ferromagnetic state and the data were taken during cooling.

The NMR experiments were performed with a Redstone-TECMAG spectrometer (10–500 MHz), which is interfaced with a power level meter and the NMR probe head (NMR-Service). The latter is equipped with computer controlled step motors, which allow fully automated tuning and matching of the tank circuit, ensuring minimal reflected *rf* signal over a very broad frequency range. The setup is supplemented by a Janis cryostat and a Lakeshore temperature controller, which allow measurements in the range 1.5–300 K. The ^{55}Mn NMR signals were obtained by a 0.8 μs-τ-0.8 μs spin-echo pulse sequence where the separation between the *rf* pulses was $\tau = 5$ μs. It is well known that, in ferromagnets, the applied *rf* field H_1 and the induced NMR signals are enhanced by a factor known as *rf* enhancement factor η (see Sec. III C 2) [43]. The NMR spectra presented here are corrected for the *rf*-enhancement factor and, thus, the relative intensities are proportional to the number of resonating nuclei at each different frequency at time 2τ. The protocol followed here is similar to Refs. [44,45]. The spin-lattice relaxation time was measured at the peak of the austenitic and martensitic spectra, by applying a saturation recovery technique and by fitting with a single exponential recovery law.

III. EXPERIMENTAL RESULTS

A. X-ray powder diffraction

Sample II. Figure 1 shows the room-temperature x-ray pattern of sample II. We find broadened reflections with different shapes, a high signal-to-noise ratio and an isotropic peak shift to higher angles. As an additional feature, a peak asymmetry located to higher angles is observed, especially for the 220, 442, and 444 reflections. Two possible scenarios may lead to this behavior: (i) textures, (ii) a second phase or a distortion of the observed cubic phase, or a concomitant overlay of both (i) and (ii). Especially the second scenario, involving a second phase, probably martensitic, seems to be

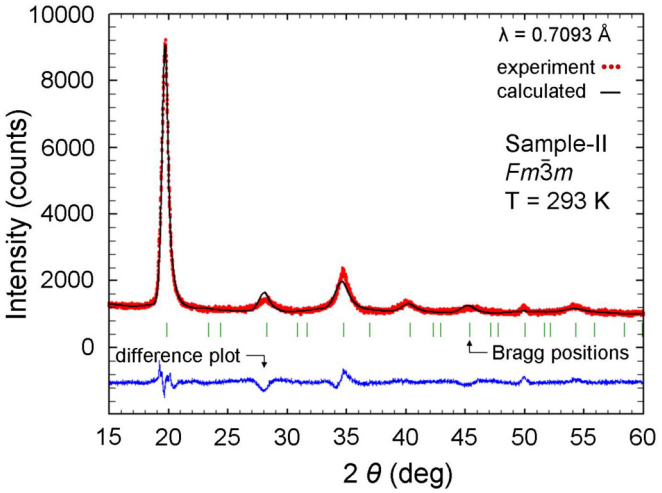

FIG. 1. (Color online) The x-ray powder diffraction pattern of sample II at 293 K.

consistent with the NMR results of sample II. The lattice parameter a for the $Fm\bar{3}m$ structure model used for refinement is determined to 5.8161(9) Å with an unit cell volume $V =$ 196.7(1) Å^3.

Sample III. Low-temperature x-ray powder diffraction was measured on a powder of sample III. The Rietveld refinements were performed with focus on phase transition, phase content and lattice parameters. All results are presented in Table I. The x-ray patterns of sample III at 293 K and 140 K are displayed in Fig. 2. The lattice parameter a of the cubic phase [$Fm\bar{3}m$, Fig. 2(a)] changes upon cooling from 5.8210(1) Å at 293 K to 5.8092(2) Å at 170 K. During warming up, a small hysteresis is observed and the lattice parameter a does not reach its initial value at 293 K. This effect is known for untrained Heusler compounds with martensitic phase transformation [2]. The onset of the martensitic phase [*Pnnm*, Fig. 2(b)] takes

TABLE I. Lattice parameters and phase contents (p.c.) of the temperature-dependent XRD experiments on sample III. The temperature regime is shown from cooling to heating.

T(K)	SG	a(Å)	b(Å)	c(Å)	V(Å^3)	p.c.
293	225	5.8210(1)			197.24(1)	
230	225	5.8139(1)			196.52(1)	
200[a]	225	5.8124(1)			196.364(2)	
180[a]	225	5.8116(1)			196.29(1)	
170[b]	225	5.8092(2)			196.05(3)	65%
	58	4.2051(7)	29.275(4)	5.5808(7)	687.0(3)	35%
140[b]	58	4.2044(4)	29.261(2)	5.5672(4)	684.9(2)	
170[b]	58	4.1969(17)	29.224(9)	5.5760(15)	683.9(7)	31%
	225	5.8045(2)			195.98(2)	69%
180[a]	225	5.8104(2)			196.17(3)	
200[a]	225	5.8121(2)			196.34(2)	
230	225	5.8125(2)			196.37(2)	
293	225	5.8176(1)			196.90(1)	

[a]*Pnnm* phase is already visible, but not refinable. All parameters were set manually.

[b]B_{ov} set to zero, otherwise becomes negative related to stress/strain or other texture effects.

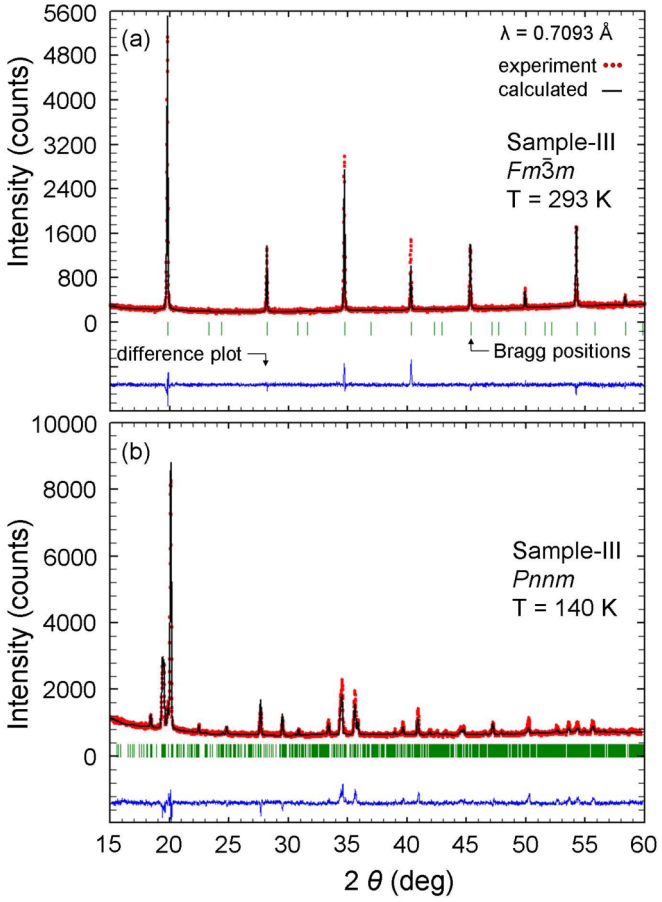

FIG. 2. (Color online) The x-ray powder diffraction patterns of sample III in (a) the austenitic ($Fm\bar{3}m$) phase at 293 K and (b) in the martensitic (*Pnnm*) phase at 140 K.

place at 200 K and finishes at 140 K, with lattice parameters of $a = 4.2044(4)$ Å, $b = 29.261(2)$ Å, and $c = 5.5672(4)$ Å. The orthorhombic 7M martensitic phase provided the best refinement for our sample, as compared to other phases (such as the monoclinic 5M structures), and was selected as the structure model [23,46]. The evolution of the phase transition is similar for the warming branch where the transition is almost completed at 200 K. Nevertheless, it has to be noted that a martensitic phase may be present at higher temperatures in both temperature cycles but it is neither refinable nor the reflections are well defined. This fact is easily demonstrated on the theoretically most intense 172 reflection, which is visible with a signal-to-noise ratio of ≈1.1. Additionally a complex microstructure of the investigated Heusler compound cannot be excluded. However, texturing may be the most probable reason for residual nonrefinable intensities.

B. Magnetization measurements

Figures 3(a)–3(f) show the ZFC/FC magnetization curves at 100 Oe for the three samples investigated in this work, while Figs. 3(d)–3(f) show the corresponding data at 4 T.

Sample I. From the low-field magnetization measurements in sample I [see Fig. 3(a)] we find a jump at $T_c = 382$ K (taken as the minimum point of dM/dT), which corresponds

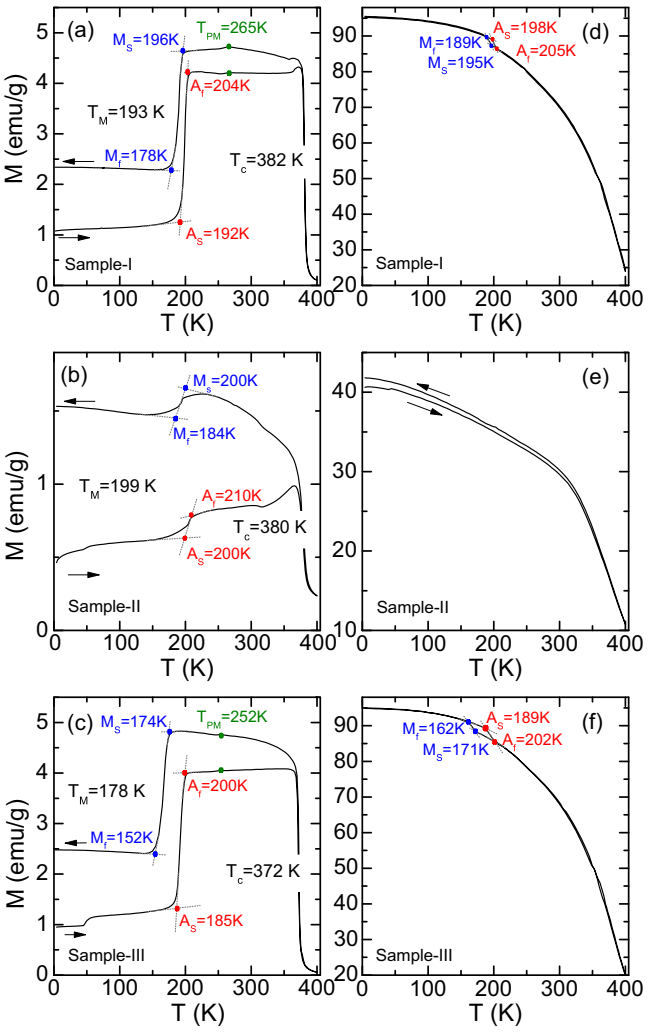

FIG. 3. (Color online) ZFC and FC magnetization loops measured at 100 Oe for samples I, II, and III in (a)–(c) respectively. The corresponding high field ($H = 4$ T) data are presented in (d)–(f).

to the transition from the PM to the FM phase. Right below T_c we observe the so-called Hopkinson peak [47]. At lower temperatures we observe a small bump at $T_{PM} = 265$ K, which is attributed to the premartensitic transition [21]. Finally, the large drop at T_M is due to the onset of the martensitic phase which, as expected, has higher magnetic anisotropy compared to the cubic austenitic phase [1]. The transition temperature T_M is estimated by $T_M = (M_s + M_f + A_s + A_f)/4$ [48], where the martensitic (austenitic) transformation temperatures upon cooling (warming) M_s (A_s), M_f (A_f) are marked in Fig. 3. The magnetic measurements performed at $H = 4$ T, which is higher than the saturating field at all temperatures, show a small increase of the magnetization by 1.8 emu/g (0.078 μ_B per formula unit) at the onset of the martensitic transition. This increase is in agreement with *ab initio* electronic structure calculations by Opeil *et al.* [34], which show a spectral weight transfer from the spin-down to the spin-up channel at the martensitic transition. Our NMR experiments presented in Sec. III C below give an independent confirmation of this fact.

Sample II. Here the transition to the ferromagnetic state occurs at $T_c = 380$ K [Fig. 3(b)], which is very close to the

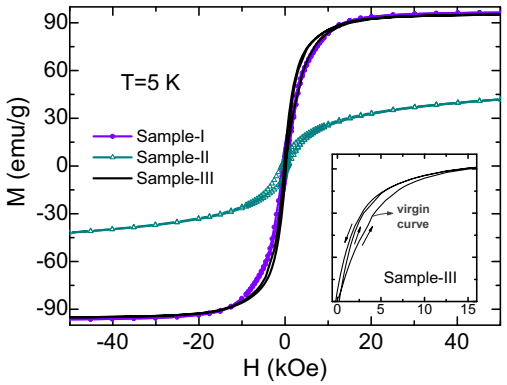

FIG. 4. (Color online) Magnetization loops at 5 K for samples I, II, and III. The inset offers a magnified view of the M-H loop for sample III.

value found in sample I. However, the jump at the martensitic transition is now much weaker and the magnetization is considerably lower in the whole temperature range. As shown by the NMR line-shape data below, this behavior is clearly not due to a lower value of the local magnetic moments. This is evident by the fact that the NMR frequency (see left panels in Fig. 6), which is proportional to the local magnetic moment, is similar for sample II to the one measured in sample I and III. Thus the behavior observed here is not due to lower local magnetic moment but due to a much larger saturation field, i.e., a much larger macroscopic anisotropy in both the austenitic and martensitic phases of sample II. The hard magnetic behavior is further reflected in the high field M-T data of Fig. 3(e) [where we also note that no anomaly is observed at T_M as in the low field data of Fig. 3(d)], and it is also evident in the magnetization process shown in Fig. 4.

The larger anisotropy is consistent with the (about two times) larger values of the so-called restoring fields that are extracted from the local NMR *rf*-enhancement measurements (see below). However, the annealed sample (sample III) has comparable restoring fields with sample II, but shows similar saturation field with sample I (modulo the demagnetizing fields). This means that the magnetic domain reorientation process of sample II is largely obstructed by defects that are created by the powderization process, and which remain robust even below the martensitic transition. Moreover, the manifestation of higher pinning due to defects is also consistent with much larger coercive fields (Fig. 4) in sample II compared to sample III.

Sample III. Here we find that the annealing treatment (Sec. II) resulted in recovering the magnetization jump at the onset of the martensitic transition, which can be observed both in low and high magnetic fields [Figs. 3(c), 3(f)]. This behavior shows that by annealing we have lowered the magnetic anisotropy and have thus eliminated the aforementioned defects. On the other hand, the transition temperatures T_c, T_{PM}, and T_M are lower in sample III compared to samples I and II, and the Hopkinson peak disappears from the low-H data. The latter implies lower magnetic anisotropy in the austenitic phase of this particular sample, which as we will see in Sec. III C is in agreement with the NMR results. Furthermore, a small downturn is observed at 55 K in the low field ZFC

data. Similar behavior has been observed in Ni-Mn-Sn [49], Ni-Mn-Sb [50], and Ni-Mn-In [51], and was attributed to coexisting FM and antiferromagnetic (AFM) phases, which gives rise to an exchange bias effect that may manifest in shifted hysteresis loops. Here, the presence of this anomaly is not accompanied by a shift in the magnetization loops and may be associated with the presence of austenitic traces down to low temperatures according to our zero-field NMR experiments presented in Sec. III C 2. We anticipate that the coexistence of martensitic and austenitic phases, which have distinct magnitude and T dependence of magnetocrystalline anisotropy, can be responsible for the small downturn observed in Fig. 3(c).

Magnetization loops. From the magnetization loops collected at $T = 5$ K (Fig. 4), we find that the magnetic moment of sample I at saturation is $M = 96$ emu/g, as in other works [1], and the anisotropy field (obtained from the anomaly in d^2M/dH^2) is $H_A = 3.5$ kOe, which is a typical value for the stoichiometric Ni_2MnGa [52–54]. In contrast, in sample II we find that an applied field of 5 T is not sufficient to saturate the magnetization, which indicates, as discussed above, that powderizing the sample induces internal strains and defects. Turning to sample III, we find that the annealing process has recovered the soft magnetic behavior and the high value of the saturation magnetization. We should note here that the data of Fig. 4 have not been corrected for the demagnetizing field, and thus a direct quantitative comparison of the anisotropy field values between sample I (bulk) and sample III (powder) is not possible. However, as already outlined above, the observation of much larger coercive fields (Fig. 4) in sample II compared to sample III reflects the presence of stronger magnetic pinning due to defects in sample II.

A noticeable feature of sample III is that the virgin magnetization curve lies below the returning loops, see inset of Fig. 4. This behavior is usually due to the magnetic field induced rearrangement of the martensitic variants in the ferromagnetic martensite [55–57]. However, we note that similar behavior has been observed in other Heusler alloys with martensitic transition such as the off-stoichiometric Ni-Mn-In [58], Ni-Mn-Sn [59], Ni-Co-Mn-Sn [60], and Ni-Co-Mn-Sb [61], as well as in several other classes of magnetic systems, which exhibit a first-order FM-AFM transition [62–65]. In these systems this behavior is attributed to the kinetic arrest of the first-order phase transition [62]. Such a possibility is also open in our case since the NMR experiments (Sec. III C 2) show the presence of austenitic traces well inside the martensitic phase.

C. Nuclear magnetic resonance

1. ^{55}Mn *NMR line shapes*

The zero-field ^{55}Mn NMR spectra were measured in the temperature range 5–297 K upon cooling for all samples and the results are presented in Fig. 5.

Sample I. At high temperatures we observe one peak, which corresponds to the austenitic phase and is indicated as P_A in Fig. 5(a). The presence of a single peak is indeed expected in well-ordered stoichiometric Heusler alloys within the $Fm\bar{3}m$ crystal structure, since there is only one Mn site with octahedral site symmetry and thus the quadrupolar splitting is zero. However a small asymmetry of the line towards low frequencies is observed. This could be explained either by the presence of a small disorder in the system, or by small deviations from the cubic structure.

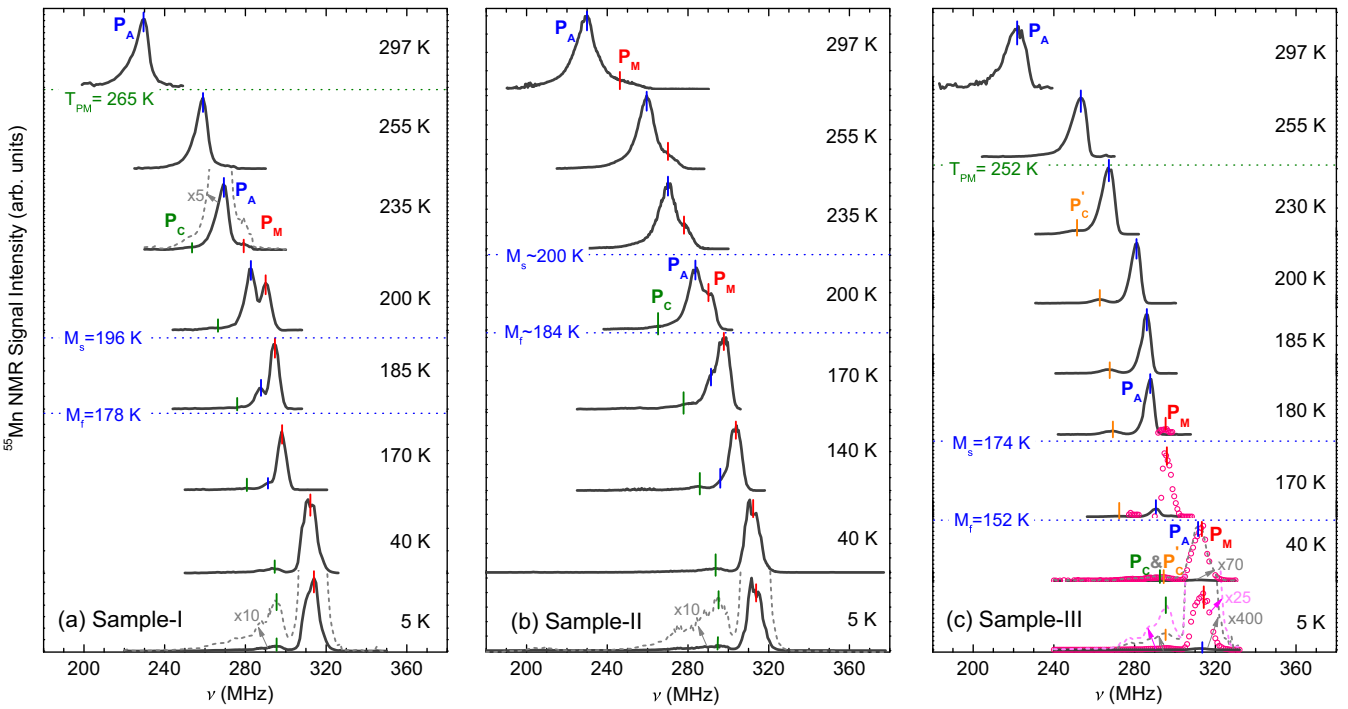

FIG. 5. (Color online) Zero-field ^{55}Mn NMR spectra of polycrystalline Ni_2MnGa samples acquired upon cooling. (a) sample I, (b) sample II, and (c) sample III at various temperatures. With dotted lines we provide enlarged views at some characteristic temperatures. The transformation temperatures obtained from the magnetization measurements are also indicated.

At $T \sim 235$ K a new peak, P_M, appears at higher frequencies compared to P_A, whose intensity grows by decreasing temperature. At the same time the intensity of the austenitic peak P_A decreases until it disappears from the spectrum at around 140 K. The peak P_M, which was first reported in Ref. [66], dominates the NMR spectrum at low temperatures and thus originates from the manganese sites in the martensitic phase of the sample. This is further supported by the *rf*-enhancement experiments presented in Sec. III C 2, which in addition shed light on the local magnetic anisotropies of austenitic and martensitic phases. It is interesting to note that the martensitic peak P_M is shifted by 8 MHz (0.762 T), compared to the austenitic peak P_A. For a typical value of the hyperfine coupling constant $A = 10\ T/\mu_B$ [67], we find that the enhancement of the hyperfine field corresponds to an increase of the magnetic moment by 0.076 μ_B in the martensitic phase. This value is in nice agreement with our high field magnetization data (Sec. III B) and with electronic structure calculations, which have shown that the martensitic transformation in Ni_2MnGa is accompanied by a spectral weight transfer from spin-down to spin-up electrons [34].

Apart from the two main peaks P_A and P_M, we also note that below 235 K the low-frequency tail of the NMR spectrum begins to develop into a small peak, which hereafter we will indicate as P_C. The peak P_C is observed down to low temperatures where its fine structure is unveiled. Specifically, apart from P_C, we can distinguish three smaller equidistant peaks at lower frequencies with an average frequency shift among them of approximately 10–15 MHz. The NMR signal from these low-frequency peaks amounts to approximately 10% of the total intensity and comes from manganese sites, which have different local environment compared to the nuclei contributing to peak P_M. In particular, the presence of these lines points to a slightly off-stoichiometric composition, of the type $Ni_2Mn_{1+x}Ga_{1-x}$, for our sample.[1] In this case, the first- and third-shell environments of the Mn atoms are unaffected (each containing 8 Ni atoms and 12 Mn atoms respectively, as in Ni_2MnGa), whereas in the second shell (6 Ga atoms in the case of Ni_2MnGa) a mixing of Mn and Ga atoms will occur. This will give rise to a maximum number of seven possible second-shell environments for the Mn atoms, such as 6 Ga, 5 Ga + 1 Mn,..., 1 Ga + 5 Mn, and 6 Mn. The relative intensities of these peaks depend upon the amount of off-stoichiometry x and can be found by applying a binomial distribution function for the probability of appearance of each particular environment (see for example Ref. [68]). By applying this model here we find a very small value of $x \sim 0.013$, which is beyond the detection limit of our energy dispersive x-ray (EDX) analysis.

We also note that even though the ^{55}Mn spin is $I = 5/2$, no quadrupole structure is apparent in the NMR spectrum inside the tetragonal phase, which shows that the quadrupole splitting is much smaller than the linewidth of the inhomogeneously broadened line (8 MHz).

[1]Other off-stoichiometric forms (for example Ni deficiency, or excess) will also give rise to multiple NMR lines, but the splitting between the lines will be either much smaller or bigger than the value observed here.

Sample II. The NMR line shapes of sample II [Fig. 5(b)] show similarities but also a few differences compared to the corresponding spectra of the parent compound. The main difference to sample I is that upon powderizing we have created traces of the martensitic phase (peak P_M) already from high temperatures. The high-frequency peak indicated as P_M in Fig. 5(b) is readily attributed to the martensitic phase, for two main reasons. At first, its resonance frequency is smoothly connected to the martensitic peak at lower temperatures, as can be seen in Fig. 6(b). The second argument comes from the *rf*-enhancement experiments presented in Sec. III C 2. The *rf* power required to excite the nuclei contributing to peak P_M at high temperatures is the same as the one applied deep inside the martensitic phase and it is clearly distinct from the typical values found in the austenitic phase of sample I. These findings imply that the stresses induced upon the sample preparation have created traces of the martensitic phase already at room temperature, which is also in line with our x-ray powder diffraction data. From the line-shape data we find that the martensitic peak accounts to 25% of the total NMR signal intensity at 297 K.

Besides the appearance of peak P_M at high T, the behavior of sample II is similar to sample I. The small peak P_C is also present here, as well as the austenitic peak P_A. Peaks P_A and P_C have similar resonance frequency and temperature dependence [Fig. 6(b)] as the corresponding peaks in sample I [Fig. 6(a)]. We note though that the full width at half maximum (FWHM) of peak P_A is larger in sample II compared to the

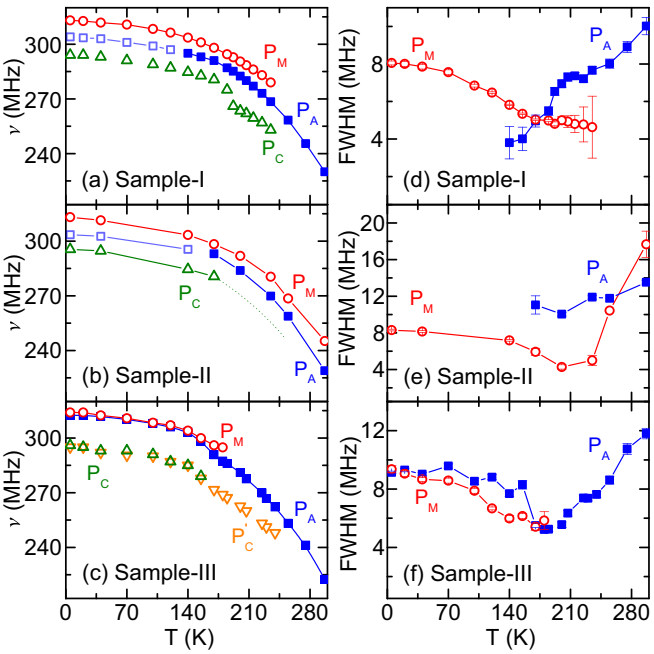

FIG. 6. (Color online) Temperature dependence of the ^{55}Mn NMR resonance frequency for the main peaks observed in (a) sample I, (b) sample II, and (c) sample III. With open squares in (a) and (b) we give the resonance frequency of austenitic remnants found at low temperatures from the *rf*-enhancement experiments presented in Sec. III C 2. The temperature dependence of the full width at half maximum (FWHM) for the austenitic peak P_A and martensitic peak P_M for (d) sample I, (e) sample II, and (f) sample III. Lines are guides to the eye.

bulk parent compound, indicating enhanced inhomogeneities (magnetic or/and structural) in the austenitic phase of the powdered sample.

Sample III. After annealing sample II, we find that the high-temperature ($T > 200$ K) signal from the martensitic phase P_M disappears. Instead, the martensitic peak P_M shows up at intermediate temperatures as found in sample I. This indicates that by annealing we have released the internal strains and eliminated the martensitic phase grown in sample II upon its powderization process. This is in agreement with our x-ray powder diffraction data and is further supported by the smaller FWHM of the austenitic peak P_A in sample III compared to sample II, which are plotted in Fig. 6(b) and 6(c) respectively. The resonance frequency for the austenitic peak P_A at high temperatures, as well as for the martensitic peak P_M for sample III [Fig. 6(c)], are slightly smaller than the corresponding values of the other samples. The intensity of the austenitic peak P_A decreases on cooling, while that of the martensitic peak P_M increases, as found in the other samples.

Sample III shows austenitic remnants down to 5 K, as can be seen in the line-shape measurements of Fig. 5(c). At low temperatures the NMR signals from austenitic and martensitic phases overlap in frequency, but the distinction between the two is still possible due to their very different *rf*-enhancement factors, see Sec. III C 2. We note here that the amount of austenitic remnants is quite low (less than 0.1%) and, thus, not possible to detect with the x-ray powder diffraction data. Apart from peaks P_A and P_M we also notice that the low-frequency tail of the lines, present at high temperatures, transforms into a small peak P'_C around 230 K [Fig. 6(c)], in a similar way with the other two samples. The peak P'_C is observed down to low temperatures where it overlaps with the much stronger martensitic peak P_C. Furthermore, as has been found in the other two samples, apart from P'_C and P_C, some weaker equidistant peaks are again observed at lower frequencies. As we discussed above, these low-frequency peaks, like P_C and P'_C, stem from the very small off-stoichiometry of our samples.

We should point out here that the temperature dependence of the FWHM of the austenitic peak P_A [Figs. 6(d)–6(f)], similar in all three samples, decreases by approaching the martensitic transition. This is not surprising close to the transition temperature (as the austenitic regions disappear in favor of the martensitic regions), but the fact that this process begins already at high temperatures indicates that the precursor phenomena take place well inside the parent phase and this can be probed by local probes such as NMR. Finally, the values of the FWHM in the low-T martensitic phase (8–10 MHz) indicate that in the modulated state the variation of the magnetic moments in the crystal structure are smaller than 0.09 μ_B, which is in line with recent theoretical predictions [69].

2. Local restoring fields

In ferromagnets the strong hyperfine field, H_{HF}, lifts the degeneracy of the nuclear energy levels and, thus, allows to perform NMR experiments without the need to apply an external static magnetic field. Under the action of the *rf*-field h_a^{rf}, the electronic magnetization oscillates and its angle of oscillation is given as h_a^{rf}/H_R, where H_R is the restoring field acting upon the magnetic moments due to the various anisotropies present in the system [44,45]. The oscillation of the electronic magnetization is directly followed by the strong hyperfine field itself, which, thus, acquires an oscillating transverse component h_{HF}^{rf}. The angle of oscillation of the hyperfine field is given as $h_{HF}^{rf}/H_{HF} = h_a^{rf}/H_R$ [44,45]. The transverse component of the hyperfine field h_{HF}^{rf} is larger than the applied *rf*-field h_a^{rf} by the so-called enhancement factor η [43–45],

$$\eta = \frac{h_{HF}^{rf}}{h_a^{rf}} = \frac{H_{HF}}{H_R}. \quad (1)$$

Thus, an independent measurement of the enhancement factor and of the hyperfine field gives direct access to the local restoring fields and allows one to obtain important information upon the magnetic stiffness in our samples. In addition, this can be done for each separate line in the NMR spectrum and thus for each different magnetic or structural environment in the system.

The enhancement factor is also important upon signal reception. The precession of the nuclear magnetization drives the precession of the electronic magnetization, and so the NMR signal intensity I(ω) (the number of nuclei in each different frequency ω) is enhanced by the same factor η, as happens upon excitation [43–45]. It has been shown that for a single-phased ferromagnetic material, and due to the omnipresent distribution of enhancement factors, the observed NMR signal intensity S(h_a^{rf},ω) will tend to the log-normal distribution [44,45],

$$S\left(h_a^{rf},\omega\right) = \eta(\omega)I(\omega)\exp\left[-\log^2\left(h_a^{rf}/h_{a,opt}^{rf}\right)/2\sigma^2\right], \quad (2)$$

where σ sets the width of the Gaussian distribution, and $h_{a,opt}^{rf}$ sets the value of the applied *rf* field, which gives the maximum signal intensity. This happens when the oscillating transverse component h_{HF}^{rf} of the hyperfine field acquires the value $h_{HF,opt}^{rf} = \pi/2\gamma\tau$, where τ is the pulse length and γ the gyromagnetic ratio [44,45].

Due to the *rf*-enhancement mechanism, the NMR sensitivity in ferromagnets is significantly improved. On the other hand special care should be taken in order to extract from the raw experimental data the actual number of nuclei in each different frequency $I(\omega)$. According to Eq. (2), this requires to measure the signal intensity by varying the amplitude of h_a^{rf} for each resonance frequency in the NMR spectrum.[2] These measurements give access to the value of $h_{HF,opt}^{rf}$ and, in turn, to the restoring field H_R via Eq. (1).

The frequency dependence of the restoring field H_R is presented in Figs. 7(a)–7(c) for some representative temperatures, while in Figs. 7(d)–7(f) we show the T dependence of the restoring fields for the main peaks observed in the NMR spectra. A first observation is that in samples I and II there is a frequency dependence of the restoring field, which implies the coexistence of magnetic environments with very distinct

[2]We note here that the NMR spectra presented in Fig. 5 are corrected for the enhancement and thus the relative intensities are proportional to the number of resonating nuclei at each different frequency at time 2τ.

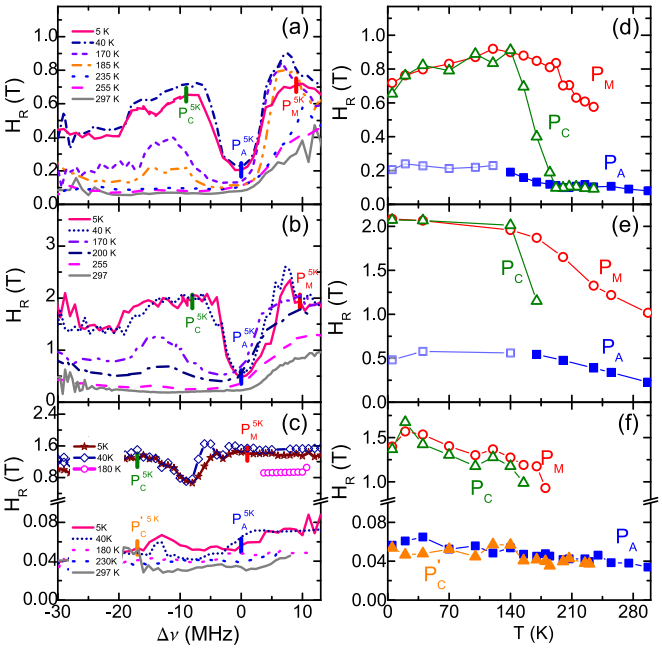

FIG. 7. (Color online) The restoring field H_R as a function of the frequency shift $\Delta\nu = \nu - \nu_o$ at various temperatures for (a) sample I, (b) sample II, and (c) sample III. The reference point, ν_o, is set to the position of the austenitic peak P_A at high temperatures, while at low temperatures as the resonance frequency where the minimum restoring field is observed. In (d)–(f) we plot the temperature dependence of the restoring field for the austenitic peak P_A, the martensitic peak P_M and the peaks P_C and P'_C for the three samples.

magnetic stiffness. In this way, NMR gives access to valuable local information on magnetic anisotropies which is otherwise not accessible from, e.g., bulk magnetization measurements, that provide only a weighted average of the anisotropy.

The frequency dependence of the restoring field becomes more evident by lowering the temperature where, in addition, a significant gradual enhancement of the restoring field is observed. The enhancement of H_R is signaling the transformation of an increasing number of austenitic regions to the low-T martensitic phase, which has higher anisotropy. The dip observed in the frequency dependence of the restoring field for samples I and II down to 5 K [Figs. 7(a), 7(b)] indicates that remnants of the high-T austenitic phase remain deep inside the martensitic phase. This behavior is supported by the fact that the resonance frequency of these regions is smoothly connected to the resonance frequency of the high-T austenitic phase as can be seen in Fig. 6, where the position of the dip is given by open symbols. We should also point out here that the amount of the low-T austenitic remnants is minute compared to the martensitic regions as can be seen in the intensity plots in Figs. 5(a) and 5(b).

Regarding the sample II, we should emphasize that the values of restoring fields and thus the local magnetic stiffness in this particular sample are generally higher compared to the other two samples. This occurs not only in the low-T martensitic phase but already from the high-T phase and indicates that the sample preparation process has created strains and precursors of the martensitic phase already at high-T. We also find that by annealing sample II (Sec. II), the strains and the martensitic remnants can be eliminated. As can be seen in Figs. 7(c), 7(f), in sample III the high-T phase is characterized by very low restoring fields and thus the annealing treatment has a large impact upon the magnetic anisotropy. Furthermore, we note that the restoring field shows a weak frequency dependence at high-T in sample III, showing a larger degree of magnetic homogeneity.

We also note that in sample III and below 180 K, the NMR signal intensity $S(h_a^{rf},\omega)$ is described by a double Gaussian distribution in h_a^{rf} instead of the high-T single Gaussian distribution of Eq. (2). The high restoring field value for the new component [Fig. 7(c)] shows that this component is martensitic. The appearance of this martensitic component at 180 K in our NMR measurements is in agreement with the magnetic measurements in Fig. 3. Finally, remnants of the austenitic phase are observed down to 5 K. The intensity of austenitic traces is negligible (less than 0.1%) compared to the martensitic phase [Fig. 5(c)] but it is higher here compared to samples I and II.

3. *Nuclear spin-lattice relaxation*

The spin-lattice relaxation rates $1/T_1$ in the austenitic and martensitic phases for sample I are presented in Fig. 8. At low temperatures, well inside the martensitic phase, the nuclear spin-lattice relaxation rate $1/T_1$ follows a linear T dependence (see inset of Fig. 8). This behavior is expected for d-band FM metals where $1/T_1$ is dominated by fluctuating orbital and dipolar interactions due to electrons at the Fermi level and is given as $1/T_1 \propto T[\rho_\uparrow(E_F)^2 + \rho_\downarrow(E_F)^2]$, where $\rho_{\uparrow(\downarrow)}(E_F)$ the density of d-band states for up (down) spins at the Fermi level [70–72]. A deviation from the linear temperature dependence is observed as we are approaching the martensitic transition, where the spin-lattice relaxation rate $1/T_1$ becomes faster.

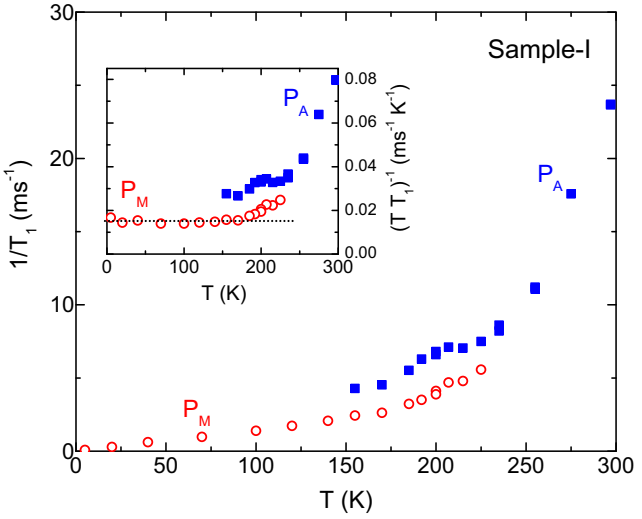

FIG. 8. (Color online) The temperature dependence of ^{55}Mn spin-lattice relaxation rate $1/T_1$ in the austenitic (squares) and the martensitic (circles) phase of bulk (sample I) Ni_2MnGa. The inset shows the spin-lattice relaxation rate data divided by temperature, $(T T_1)^{-1}$, as a function of temperature.

In addition, we find that the spin-lattice relaxation rate $1/T_1$ is lower in the martensitic phase compared to the austenitic phase in the temperature region where the two phases coexist. This behavior indicates lower density of states at the Fermi level for the martensitic phase compared to the austenitic phase. This result is supporting ultraviolet-photoemission (UPS) measurements, which show redistribution in the intensity of the UPS spectra at both the premartensitic and martensitic transitions [34,35].

IV. SUMMARY

We have studied bulk and powder samples of the Heusler shape-memory alloy Ni_2MnGa with zero-field static and dynamic ^{55}Mn NMR experiments, x-ray powder diffraction, and magnetization experiments.

The sequence of structural phase transitions in or samples was tracked from the high-T austenitic phase down to the low-T martensitic phase. Zero-field ^{55}Mn NMR line-shape measurements provide the T dependence of the local hyperfine fields, i.e., the T dependence of the local magnetic moments, in austenitic and martensitic phases. The onset of the martensitic signal at temperatures higher than those indicated by the bulk magnetization measurements, as well as the T dependence of the FWHM of the austenitic peak show that the precursor phenomena start well inside the parent austenitic phase. In addition, we have resolved differences in magnetic spin moments of the two phases of the order of 0.08 μ_B and we have detected austenitic traces inside the martensitic phase that are too small to be observed easily with other methods. By NMR *rf*-enhancement experiments, we have measured the frequency-resolved restoring fields, which provide the local magnetic anisotropy of each different structural environment in our samples. In doing this, we are able to differentiate signals coming from austenitic and martensitic components and provide the T dependence of the local magnetic stiffness in each phase. Furthermore, the T dependence of the zero-field ^{55}Mn NMR spin-lattice relaxation rates was measured for both austenitic and martensitic phases. The results show that the density of states at the Fermi level is lowered upon entering the martensitic phase. We also find that sample preparation has a strong impact on the weight of the austenitic and martensitic components in each temperature region. Specifically, we show that powderization gives rise to a significant portion of martensitic traces inside the high-T austenitic region, and that these traces can be subsequently removed by annealing.

ACKNOWLEDGMENTS

We acknowledge experimental assistance from K. Leger, S. Müller-Litvanyi, A. Omar, and M. Gellesch and fruitful discussions with I. Rousochatzakis. S.W. acknowledges funding by Deutsche Forschungsgemeinschaft DFG in Project WU 595/3-1.

[1] P. J. Webster, K. R. A. Ziebeck, S. L. Town, and M. S. Peak, Philos. Mag. B **49**, 295 (1984).
[2] A. N. Vasil'ev, V. D. Buchel'nikov, T. Takagi, V. V. Khovailo, and É. I. Éstrin, Phys. Usp. **46**, 559 (2003).
[3] P. Entel, V. D. Buchelnikov, V. V. Khovailo, A. T. Zayak, W. A. Adeagbo, M. E. Gruner, H. C. Herper, and E. F. Wassermann, J. Phys. D: Appl. Phys. **39**, 865 (2006).
[4] K. Ullakko, J. K. Huang, C. Kantner, R. C. O'Handley, and V. V. Kokorin, Appl. Phys. Lett. **69**, 1966 (1996).
[5] F. X. Hu, B. G. Shen, and J. R. Sun, Appl. Phys. Lett. **76**, 3460 (2000).
[6] C. Biswas, R. Rawat, and S. R. Barman, Appl. Phys. Lett. **86**, 202508 (2005).
[7] J. Kübler, A. R. Williams, and C. B. Sommers, Phys. Rev. B **28**, 1745 (1983).
[8] A. Zheludev, S. M. Shapiro, P. Wochner, A. Schwartz, M. Wall, and L. E. Tanner, Phys. Rev. B **51**, 11310 (1995).
[9] S. M. Shapiro, Y. Noda, Y. Fujii, and Y. Yamada, Phys. Rev. B **30**, 4314 (1984).
[10] S. M. Shapiro, B. X. Yang, Y. Noda, L. E. Tanner, and D. Schryvers, Phys. Rev. B **44**, 9301 (1991).
[11] G.-L. Zhao, T. C. Leung, B. N. Harmon, M. Keil, M. Müllner, and W. Weber, Phys. Rev. B **40**, 7999 (1989).
[12] G. L. Zhao and B. N. Harmon, Phys. Rev. B **45**, 2818 (1992).
[13] Y. Lee, J. Y. Rhee, and B. N. Harmon, Phys. Rev. B **66**, 054424 (2002).
[14] C. Bungaro, K. M. Rabe, and A. Dal Corso, Phys. Rev. B **68**, 134104 (2003).
[15] A. T. Zayak, P. Entel, J. Enkovaara, A. Ayuela, and R. M. Nieminen, Phys. Rev. B **68**, 132402 (2003).
[16] A. Planes, E. Obradó, A. Gonzàlez-Comas, and L. Mañosa, Phys. Rev. Lett. **79**, 3926 (1997).
[17] M. A. Uijttewaal, T. Hickel, J. Neugebauer, M. E. Gruner, and P. Entel, Phys. Rev. Lett. **102**, 035702 (2009).
[18] A. Zheludev, S. M. Shapiro, P. Wochner, and L. E. Tanner, Phys. Rev. B **54**, 15045 (1996).
[19] J. Worgull, E. Petti, and J. Trivisonno, Phys. Rev. B **54**, 15695 (1996).
[20] T. E. Stenger and J. Trivisonno, Phys. Rev. B **57**, 2735 (1998).
[21] F. Zuo, X. Su, and K. H. Wu, Phys. Rev. B **58**, 11127 (1998).
[22] P. J. Brown, J. Crangle, T. Kanomata, M. Matsumoto, K.-U. Neumann, B. Ouladdiaf, and K. R. A. Ziebeck, J. Phys.: Condens. Matter **14**, 10159 (2002).
[23] L. Righi, F. Albertini, G. Calestani, L. Pareti, A. Paoluzi, C. Ritter, P. A. Algarabel, L. Morellon, and M. R. Ibarra, J. Solid State Chem. **179**, 3525 (2006).
[24] V. V. Martynov and V. V. Kokorin, J. Phys. III (France) **2**, 739 (1992).
[25] S. O. Mariager, T. Huber, and G. Ingold, Acta Mater. **66**, 192 (2014).
[26] S. Singh, V. Petricek, P. Rajput, A. H. Hill, E. Suard, S. R. Barman, and D. Pandey, Phys. Rev. B **90**, 014109 (2014).
[27] U. Gaitzsch, S. Roth, B. Rellinghaus, and L. Schultz, J. Magn. Magn. Mater. **305**, 275 (2006).
[28] U. Gaitzsch, M. Pötschke, S. Roth, N. Mattern, B. Rellinghaus, and L. Schultz, J. Alloys Compd. **443**, 99 (2007).

[29] S. Fujii, S. Ishida, and S. Asano, J. Phys. Soc. Jpn. **58**, 3657 (1989).

[30] P. J. Brown, A. Y. Bargawi, J. Crangle, K.-U. Neumann, and K. R. A. Ziebeck, J. Phys.: Condens. Matter **11**, 4715 (1999).

[31] A. Ayuela, J. Enkovaara, and R. M. Nieminen, J. Phys.: Condens. Matter **14**, 5325 (2002).

[32] S. R. Barman, S. Banik, and A. Chakrabarti, Phys. Rev. B **72**, 184410 (2005).

[33] S. M. Shapiro, P. Vorderwisch, K. Hradil, and H. Schneider, Europhys. Lett. **77**, 56004 (2007).

[34] C. P. Opeil, B. Mihaila, R. K. Schulze, L. Mañosa, A. Planes, W. L. Hults, R. A. Fisher, P. S. Riseborough, P. B. Littlewood, J. L. Smith, and J. C. Lashley, Phys. Rev. Lett. **100**, 165703 (2008).

[35] S. W. D'Souza, A. Rai, J. Nayak, M. Maniraj, R. S. Dhaka, S. R. Barman, D. L. Schlagel, T. A. Lograsso, and A. Chakrabarti, Phys. Rev. B **85**, 085123 (2012).

[36] A. G. Khachaturyan, S. M. Shapiro, and S. Semenovskaya, Phys. Rev. B **43**, 10832 (1991).

[37] S. Kaufmann, U. K. Rößler, O. Heczko, M. Wuttig, J. Buschbeck, L. Schultz, and S. Fähler, Phys. Rev. Lett. **104**, 145702 (2010).

[38] H. M. Rietveld, J. Appl. Cryst. **2**, 65 (1969).

[39] T. Roisnel and J. Rodriguez-Carjaval, Mater. Sci. Forum **378–381**, 118 (2001).

[40] J. Soltys, Acta Phys. Polon. A **47**, 521 (1975).

[41] P. J. Brown, A. P. Gandy, T. Kanomata, M. Matsumoto, K. Neumann, K.-U. Neumann, A. Sheikh, and K. R. A. Zieback, Mater. Sci. Forum **583**, 285 (2008).

[42] P. Thompson, D. E. Cox, and J. B. Hastings, J. Appl. Cryst. **20**, 79 (1987).

[43] A. C. Gossard and A. M. Portis, Phys. Rev. Lett. **3**, 164 (1959).

[44] P. Panissod, M. Malinowska, E. Jedryka, M. Wojcik, S. Nadolski, M. Knobel, and J. E. Schmidt, Phys. Rev. B **63**, 014408 (2000).

[45] P. Panissod, in *Magnetism: Molecules to Materials III*, edited by J. S. Miller and M. Drillon (Wiley-VCH, Weinheim, 2001), pp. 297–327.

[46] I. Glavatskyy, N. Glavatska, I. Urubkov, J.-U. Hoffman, and F. Bourdarot, Mater. Sci. Eng. A **481–482**, 298 (2008).

[47] J. Wang, C. Jiang, R. Techapiesancharoenkij, D. Bono, S. M. Allen, and R. C. O'Handley, J. Appl. Phys. **106**, 023923 (2009).

[48] A. Lakhani, S. Dash, A. Banerjee, P. Chaddah, X. Chen, and R. V. Ramanujan, Appl. Phys. Lett. **99**, 242503 (2011).

[49] Z. Li, C. Jing, J. Chen, S. Yuan, S. Cao, and J. Zhang, Appl. Phys. Lett. **91**, 112505 (2007).

[50] M. Khan, I. Dubenko, S. Stadler, and N. Ali, Appl. Phys. Lett. **91**, 072510 (2007).

[51] B. M. Wang, Y. Liu, L. Wang, S. L. Huang, Y. Zhao, Y. Yang, and H. Zhang, J. Appl. Phys. **104**, 043916 (2008).

[52] R. Tickle and R. D. James, J. Magn. Magn. Mater. **195**, 627 (1999).

[53] S.-Y. Chu, A. Cramb, M. De Graef, D. Laughlin, and M. E. McHenry, J. Appl. Phys. **87**, 5777 (2000).

[54] F. Albertini, L. Morellon, P. A. Algarabel, M. R. Ibarra, L. Pareti Z. Arnold, and G. Calestani, J. Appl. Phys. **89**, 5614 (2001).

[55] O. Heczko, L. Straka, N. Lanska, K. Ullakko, and J. Enkovaara, J. Appl. Phys. **91**, 8228 (2002).

[56] J.-M. Wang, Y.-T. Wang, C.-B. Jiang, and H.-B. Xu, Chin. Phys. Lett. **23**, 1293 (2006).

[57] N. Okamoto, T. Fukuda, T. Kakeshita, and K. Kishio, Mater. Sci. Forum **475–479**, 2021 (2005).

[58] V. K. Sharma, M. K. Chattopadhyay, and S. B. Roy, Phys. Rev. B **76**, 140401(R) (2007).

[59] S. Chatterjee, S. Giri, S. Majumdar, and S. K. De, Phys. Rev. B **77**, 012404 (2008).

[60] A. Banerjee, S. Dash, A. Lakhani, P. Chaddah, X. Chen, and R. V. Ramanujan, Solid State Commun. **151**, 971 (2011).

[61] A. K. Nayak, K. G. Suresh, and A. K. Nigam, J. Appl. Phys. **108**, 063915 (2010).

[62] S. B. Roy, J. Phys.: Condens. Matter **25**, 183201 (2013).

[63] M. A. Manekar, S. Chaudhary, M. K. Chattopadhyay, K. J. Singh, S. B. Roy, and P. Chaddah, Phys. Rev. B **64**, 104416 (2001).

[64] M. Manekar, S. Chaudhary, M. K. Chattopadhyay, K. J. Singh, S. B. Roy, and P. Chaddah, J. Phys.: Condens. Matter **14**, 4477 (2002).

[65] P. Kushwaha, R. Rawat, and P. Chaddah, J. Phys.: Condens. Matter **20**, 022204 (2008).

[66] K. Ooiwa, K. Endo, and A. Shinogi, J. Magn. Magn. Mater. **104–107**, 2011 (1992).

[67] H. Akai, M. Akai, S. Blügel, B. Drittler, H. Ebert, K. Terakura, R. Zeller, and P. H. Dederichs, Prog. Theor. Phys. Suppl. **101**, 11 (1990).

[68] S. Wurmehl, J. T. Kohlhepp, H. J. M. Swagten, B. Koopmans, C. G. F. Blum, V. Ksenofontov, H. Schneider, G. Jakob, D. Ebke, and G. Reiss, J. Phys. D: Appl. Phys. **42**, 084017 (2009).

[69] N. Xu, J.-M. Raulot, Z. Li, J. Bai, Y. Zhang, X. Zhao, L. Zuo, and C. Esling, Appl. Phys. Lett. **100**, 084106 (2012).

[70] Y. Obata, J. Phys. Soc. Jpn. **18**, 1020 (1963).

[71] T. Moriya, J. Phys. Soc. Jpn. **19**, 681 (1964).

[72] P. L. Kuhns, M. J. R. Hoch, A. P. Reyes, W. G. Moulton, L. Wang, and C. Leighton, Phys. Rev. Lett. **96**, 167208 (2006).